CHAPTER 9

A FIRST-PRINCIPLE, PHYSICS-BASED WATERSHED MODEL: WASH123D

GOUR- TSYH YEH[1], GUOBIAO HUANG[2], HWAI-PING CHENG[3], FAN ZHANG[1], HSIN-CHI LIN[3], EARL EDRIS[3], AND DAVID RICHARDS[3]

The approaches to watershed-scale modeling can be classified into three broad groups: parametric methods, stochastic approaches, and physics-based mathematical models. In the past 30 years, the watershed modeling communities have employed parametric-based models (the most famous one is the HSPF [1]; all other parametric models are similar to HSPF, e.g., SWMM [2], CREAMS [3], STORM [4], ANSWERS [5], SWRRBWQ [6]) for watershed management and assessment including ecological exposure assessments and TMDL calculations. Evolved from the pioneer model STANFORD WATERSHED IV [7], HSPF has dominated watershed simulations for more than 20 years. Physics-based, process-level chemical transport and hydrological models have been practically nonexistent until recently. It is easy to understand that only the physics-based, process-level fluid flow and thermal, salinity, sediment, and biogeochemical transport models have the potential to further the understanding of the fundamental biological, chemical and physical factors that take place in nature. It is precise for this reason that EPA ecological research strategies [8] had clearly stated that the first-principle, physics-based models should be used in ecological system assessment on a watershed scale.

Progresses in the development of first-principle, physics-based models for individual processes of infiltration, evapotranspiration, recharge, moisture redistribution in vadose zone, groundwater flow, surface runoff, and river flow have been remarkable. These individual processes must be dynamically coupled over various spatial and temporal scales. In the past, each individual process was often investigated assuming other coupling and influencing processes were *a priori*. For example, to model overland flow (surface runoff), it was often implicitly assumed that the infiltration was known and the feedback from groundwater flow and river flow were not explicitly enforced. Integrated approaches to modeling coupled processes have gained momentum recently. Many integrated models have achieved the coupling via external or internal linkage of individual process level models. As a result, these models often have to introduce undue empiricism.

This chapter specifically focuses on a first-principle, physics-based model, WASH123D [9]. The development of an integrated numerical model of the aforementioned processes is presented. A rigorous coupling of these hydrological and biogeochemical processes is achieved by imposing the continuity of fluxes and state variables. In this integrated model, any process between two media is the natural consequence of interaction and feedback between processes occurring in individual

[1] Dept of Civil and Environ. Eng., Univ. of Central Florida, Orlando, FL 32816 (gyeh@mail.ucf.edu)

[2] Dept. of Civil and Environ. Eng., Penn State, University Park, PA 16082

[3] Engineering Research and Development Center, US Army Corps of Engineer, Vicksburg, MS 39180

media. For example, infiltration and recharge are spatially and temporally varied and are the consequence of interacting flow processes on the land surface (overland) and in the subsurface media and rivers. The theoretical bases are heuristically derived. Numerical implementations of the theoretical coupling are conceptually and briefly discussed. Particular features of WASH123D in the treatment of interactions among media interfaces, the inclusion of various types of control structures and pumps, the formulation of reaction-based water quality simulations, and the implementation of optional hydrodynamics in river network and overland regime are addressed. The design capability and demonstrative examples ranging from minutes to years in temporal scale and from meters to tens of kilometers in spatial scales are presented. The potential applications of the model to watershed modeling for various temporal and spatial scales are emphasized.

I. INTRODUCTION

This chapter presents the development of a first-principle, physics-based watershed model. A watershed includes an overland regime including management structures such as storage ponds, pumping stations, culverts, and levees; a river/stream/canal network including natural junctions and control structures such as weirs, gates, culverts, and pumping; and subsurface media including management devices such as pumping and injecting wells, drainage pipes, and drainage channels. The model is composed of hydrologic and hydraulic flow, thermal and salinity transport, and reactive water quality transport.

Three options are included in modeling flow on the land surface and in river/stream/canal networks: kinematic-wave, diffusion-wave, and dynamic-wave approaches. Flow through subsurface media is described by the Richards equation where vadose and saturated zones are considered a unified media system.

Transport equations based on the principle of energy and mass balance are used to describe temporal-spatial distributions of temperature, salinity, suspended and bed sediments, and water qualities. A generic paradigm using reaction-based approaches is employed to model biogeochemical processes. In this paradigm, the system is completely defined with a reaction network. The reaction network is diagonalized with the Gauss-Jordan decomposition so that a linearly independent reaction is measured by a kinetic variable.

For surface water flow simulations, the numerical method that is most appropriate for a particular approach is used. In kinematic-wave approaches, the semi-Lagrangian method (backward particle tracking) is used to numerically approximate the kinematic-wave equation. In the diffusive wave approach, either the Galerkin finite element method or the semi-Lagrangian method is employed to numerically solve the diffusion equation governing the transport of water surface elevation. In the fully dynamic-wave approach, the primitive continuity and momentum equations are transformed into characteristic wave equations and the hybrid Lagrangin-Eulerian finite element method is applied to approximate these equations in a finite element discretization. Thus, first water depth and velocity are computed with the backward method of characteristics. Then the Galerkin finite element method is applied to the Lagrangian form of eddy-diffusion

equation. For subsurface flow simulations, the Galerkin finite element method is used to discretize the Richards equation. The Picard method is applied to deal with the nonlinearity of flow equations.

For transport simulations (including thermal, salinity, sediment, and water quality), two options are provided to discretize the governing sediment and biogeochemical transport equations: hybrid Lagrangian-Eulerian finite element methods or conventional finite element methods. The fully implicit sequential iteration approach, the operator splitting method, and the mixed predictor-corrector and operator-splitting scheme are employed to handle the coupling between the hydrologic transport and biogeochemical reactions. The Newton-Raphson method is used to solve the set of algebraic equations and ordinary differential equations describing the evolution of all biogeochemical species.

Several example problems are presented to demonstrate the design capability of the model. These problems have varied spatial-temporal scales, ranging from minutes to years and from meters to tens of kilometers.

II. MATHEMATICAL BASIS

In this section, we give governing equations, initial conditions, and boundary conditions for simulating density-dependent flow and sediment transport and reactive biogeochemical transport in watershed systems.

A. One-Dimensional River/Stream/Canal Networks.

The governing equations to simulate density-dependent flow in a river/stream/canal network include one-dimensional St Venant equations and thermal and salinity transport equations. These equations can be derived based on the conservation law of water mass, linear momentum, energy, and material mass [10], as described below.

St Venant Equations. The St Venant equations for one-dimensional flows in a river/stream/canal network include one continuity equation and one momentum equation. The continuity equation is derived based on the conservation of water mass,

$$\frac{\partial A}{\partial t}+\frac{\partial Q}{\partial x}=S^a+S^r-S^e-S^g+S^{o1}+S^{o2} \tag{9.1}$$

where t is the time [t]; x is the axis along the river/stream/canal direction [L]; A is the cross-sectional area [L^2]; Q is the flow rate [L^3/t]; S^a is the man-induced artificial source [L^3/t/L]; S^r is the source due to rainfall [L^3/t/L]; S^e is the sink due to evapotranspiration [L^3/t/L]; S^g is the sink due to groundwater infiltration [L^3/t/L]; S^{o1} and S^{o2} are the source terms contributed from overland flow from bank side 1 and 2, respectively [L^3/t/L].

The momentum equation is derived based on the conservation of linear momentum,

$$\begin{aligned}&\frac{\partial Q}{\partial t}+\frac{\partial VQ}{\partial x}=\\&-gA\frac{\partial\left(Z_O+h\right)}{\partial x}-\frac{gAh}{c\rho}\frac{\partial\Delta\rho}{\partial x}-\frac{\partial F}{\partial x}+\left(M^a+M^r-M^e-M^g+M^{o1}+M^{o2}\right)+\frac{B\tau^s-P\tau^b}{\rho}\end{aligned} \tag{9.2}$$

where V is the velocity [L/t]; g is the gravity constant [L/t^2]; Z_o is the bottom elevation [L]; h is the water depth [L]; $\Delta\rho = \rho - \rho_o$ is the density deviation from the reference density (ρ_o), which is a function of temperature and salinity as well as other chemical concentrations; c is the shape factor of the cross-sectional area; F is the momentum flux due to eddy viscosity [L^4/t^2]; M^a is the external momentum-impulse from artificial sources/sinks [L^4/t^2/L]; M^r is the momentum-impulse gained from rainfall [L^4/t^2/L]; M^e is the momentum-impulse lost to evapotranspiration [L^4/t^2/L]; M^g is the momentum-impulse lost to the groundwater due to infiltration [L^4/t^2/L]; M^{o1} and M^{o2} are the momentum-impulse gained from the overland flow [L^4/t^2/L] through river banks 1 and 2; ρ is water density [M/L^3]; B is the top width of the cross-sectional area [L]; τ^s is surface shear stress [M/t^2/L]; P is the wetted perimeter [L]; and τ^b is bottom shear stress [M/t^2/L], which can be assumed proportional to the flow rate as $\tau^b/\rho = \kappa V^2$ where $\kappa = gn^2/R^{1/3}$ and R is the hydraulic radius (L) and n is the Manning's roughness coefficient.

1. Fully Dynamic Wave Approaches

Equations (9.1) and (9.2) written in conservative form are the governing equations for one-dimensional flow in river/stream/canals. Depending on the simplification of the momentum equation, one can have three approaches: fully dynamic wave, diffusive wave, and kinematic wave. For the fully dynamic wave approach, all terms in Eq. (9.2) are retained. Under such circumstances, the conservative form of the governing equations may be used or they may be cast in the advection form or in the characteristic form. In this chapter the characteristic form of the fully dynamic approach will be used because it is the most natural way and amenable to the advective numerical methods, e.g., the upstream approximation or the Lagrangian-Eulerian method. The characteristic form of the St Venant equations can be written as [9]

$$\frac{D_{V+c}(V+\omega)}{D\tau} \equiv \frac{\partial(V+\omega)}{\partial t} + (V+c)\frac{\partial(V+\omega)}{\partial x} = \frac{g}{c}R_1 + R_2 + D \tag{9.3}$$

$$\frac{D_{V-c}(V-\omega)}{D\tau} \equiv \frac{\partial(V-\omega)}{\partial \tau} + (V-c)\frac{\partial(V-\omega)}{\partial \tau} = -\frac{g}{c}R_1 + R_2 + D \tag{9.4}$$

in which

$$c = \sqrt{\frac{gA}{B}}; \quad \omega = \int_0^h \frac{g}{c(s)}ds; \quad D = -\frac{1}{A}\frac{\partial F}{\partial x} = \frac{1}{A}\frac{\partial}{\partial x}\left(A\varepsilon\frac{\partial V}{\partial x}\right) \text{ and } F = -A\varepsilon\frac{\partial V}{\partial x} \tag{9.5}$$

$$R_1 = \frac{1}{B}\left(S^a + S^r - S^e - S^g + S^{o1} + S^{o2}\right) - \frac{V}{B}\frac{\partial A^{\#}}{\partial x} \tag{9.6}$$

$$R_2 = -g\frac{\partial Z_0}{\partial x} - \frac{gh}{c\rho}\frac{\partial(\Delta\rho)}{\partial x} + \frac{1}{A}\left[\begin{array}{l} -V\left(S^a + S^r - S^e - S^g + S^{o1} + S^{o2}\right) + \\ \left(M^a + M^r - M^e - M^g + M^{o1} + M^{o2}\right) + \dfrac{B\tau^s - P\tau^b}{\rho} \end{array}\right] \tag{9.7}$$

where $A^{\#}$ is a function of the water depth $h(x,t)$ and the axis along the river/stream/canal direction x. Equation (9.3) simply states that the positive gravity wave ($V + \omega$) is advected by the speed ($V + c$) while Equation (9.4) states that the negative gravity wave ($V - \omega$) is advected by the speed ($V - c$).

The system of Eq. (9.3) and (9.4) is identical to the system of Eq. (9.1) and (9.2) on the differential level. They offer advantages in their amenability to innovative advective

numerical methods such as the upstream finite difference, upwind finite element, or semi-Lagrangian scheme. Furthermore, the implementation of boundary conditions is very straightforward. Only when the wave is coming into the region of interest, the boundary condition is required. For the wave that is going out of the region of interest, there is no need to specify a boundary condition.

For transient simulations, water depth (or water stage) and the cross-sectionally averaged velocity must be given as initial condition. In addition, appropriate boundary conditions need to be specified to match the corresponding physical system. A total of six types of boundary conditions can be specified. They correspond to (1) open upstream boundary, (2) open downstream boundary, (3) closed upstream boundary, (4) closed downstream boundary, (5) internal boundaries at all junctions, and (6) internal boundaries at all control structures. The setup of governing equations for all global boundaries and internal boundaries can be found elsewhere [9].

2. Diffusive Wave Approaches

In a diffusive wave approach, the inertia terms in the momentum equation is assumed negligible when compared with the other terms. By further assuming negligible eddy viscosity and $M^a = M^r = M^e = M^g = M^{o1} = M^{o2} = 0$, we approximate the river/stream/canal velocity with the following equation [11],

$$V = \frac{-a}{n}\left[\frac{R}{1+\left(\frac{\partial Z_0}{\partial x}\right)^2}\right]^{2/3} \frac{1}{\sqrt{\left|\frac{\partial H}{\partial x} - \frac{h}{c\rho}\frac{\partial \Delta\rho}{\partial x} + \frac{B\tau^S}{Ag\rho}\right|}}\left(\frac{\partial H}{\partial x} + \frac{h}{c\rho}\frac{\partial \Delta\rho}{\partial x} - \frac{B\tau^S}{Ag\rho}\right) \qquad (9.8)$$

where n is the Manning's roughness coefficient [t/L$^{1/3}$], a is a unit-dependent factor (a = 1 for SI units and a = 1.49 for U.S. Customary units) to make the Manning's roughness coefficient unit-independent, R is hydraulic radius [L], and $H = h + Z_o$ is the water surface elevation. Using the definition $Q = VA$ and substituting Eq. (9.8) into Eq. (9.1), we obtain

$$B\frac{\partial H}{\partial t} - \frac{\partial}{\partial x}\left(K\left[\frac{\partial H}{\partial x} + \frac{h}{c\rho}\frac{\partial \Delta\rho}{\partial x} - \frac{B\tau^s}{Ag\rho}\right]\right) = S^a + S^r - S^e - S^g + S^{o1} + S^{o2} \qquad (9.9)$$

in which

$$K = \frac{a\,A\,R^{2/3}}{n}\frac{1}{\left[1+\left(\frac{\partial Z_o}{\partial x}\right)^2\right]^{2/3}}\frac{1}{\sqrt{\left|\frac{\partial H}{\partial x} - \frac{h}{c\rho}\frac{\partial \Delta\rho}{\partial x} + \frac{B\tau^s}{Ag\rho}\right|}} \qquad (9.10)$$

To achieve transient simulations, either water depth or stage must be given as the initial condition. In addition, appropriate boundary conditions need to be specified to match the corresponding physical system. Five types of boundary conditions may be specified depending on physical configurations of the boundary. These boundary conditions are addressed below.

The first type of boundary conditions is the Dirichlet boundary condition. On a Dirichlet boundary, either the water depth or stage can be prescribed as a function of

time. The second type is the flux boundary condition. On a flux boundary, a time-dependent flow rate is prescribed as a function of time. The third type is the water-depth dependent condition, where a prescribed rating curve must be given. This condition is often used to describe the flow rate at a downstream river/stream/canal boundary at which the flow rate is a function of water depth [9].

The fourth type of boundary condition is internal boundaries at junctions. This condition is applied to a boundary of a river/stream/canal reach that is connected to a junction (Fig. 9.1). For the junction complex consisting of *NJ* river/stream/canal reaches (e.g., in Fig. 9.1, *NJ* = 3) and one junction (say *J*), we have (*NJ* + 1) unknowns, which are flow rates, Q_{IJ} (Q_{IJ} is the flow rate from the *I*-th reach to junction J), and water stage at junction *J*, H_J. Therefore, we need to set up (*NJ* + 1) equations. The first equation is obtained by applying the continuity of mass at the junction to result in

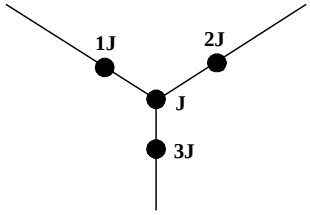

Fig. 9.1. A River Junction

$$\frac{dV_J}{dh_J}\frac{dh_J}{dt} = \sum_I^{N_J} Q_{IJ} = \sum_I^{N_J} V_{IJ} A_{IJ} \tag{9.11}$$

for the case when the storage effect of the junction must be accounted for or

$$\sum_I^{N_J} Q_{IJ} = \sum_I^{N_J} V_{IJ} A_{IJ} = 0 \tag{9.12}$$

when this effect is negligible. The other *NJ* equations can be obtained by assuming that the kinetic energy in the junction is negligible to result in

$$\frac{1}{2g}\left(\frac{Q_{IJ}}{A_{IJ}}\right)^2 + H_{IJ} = H_J, \quad I \in N_J \quad where \quad Q_{IJ} = -K\left(\frac{\partial H}{\partial x} + \frac{h}{c\rho}\frac{\partial \Delta\rho}{\partial x} - \frac{B\tau^s}{Ag\rho}\right)\Big|_{IJ} \tag{9.13}$$

where H_{IJ} is the water stage at the internal boundary node *IJ* of the *I*-th reach connecting to junction *J*. Equations (9.11) or (9.12) along with Eq. (9.13) provide (*NJ* + 1) equations to solve for (*NJ* + 1) unknowns.

The fifth type of boundary conditions is the internal boundaries adjacent to structures (weir, gate, culvert, etc.). For any structure (S), there are two river/stream/canal reaches connecting to it. The node *1S* located just upstream of the structure is termed the controlled-internal boundary of the upstream reach while the node *2S* located just downstream of the structure is called the controlled-internal boundary of the downstream reach (Fig. 9.2). Specification of boundary conditions for the internal boundaries for the diffusive wave approach is given as

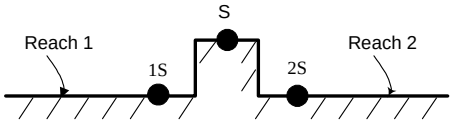

Fig. 9.2 A Ccontrol Structure

$$-\mathbf{n}\cdot\mathrm{K}\left(\nabla H + \frac{h}{c\rho}\nabla(\Delta\rho) - \frac{B\tau^s}{Ag\rho}\right)\Big|_{1S} = Q_S\left(h_{up}, h_{dn}\right) = -\mathbf{n}\cdot\mathrm{K}\left(\nabla H + \frac{h}{c\rho}\nabla(\Delta\rho) - \frac{B\tau^s}{Ag\rho}\right)\Big|_{2S} \tag{9.14}$$

where Q_S is the discharge over the structure, which is a given function of water depths h_{up} at Node *1S* and h_{dn} at Node *2S*. The flow configuration around a structure and its surrounding reaches may be very dynamic under transient flows. Both of the water stages at nodes *1S* and *2S* may be below the structure; both may be above the structure; or

one below the structure while the other is above the structure. When both stages are below the height of the structure, the two reaches connecting the structure are decoupled. When at least one of the stages is above the structure, two reaches are coupled via the structure discharge. The structure discharge, Q_S, can be obtained by solving the continuity and Bernoulli equation between Nodes *1S* and *2S*. The discharge formulae for a variety of structures under various stage conditions were given elsewhere [9].

3. Kinematic Wave Approaches

In a kinematic approach, all the assumptions for the diffusive approach hold. However, the velocity is given by a modified Eq. (9.8) with $\partial Z_o/\partial x$ replacing $\partial H/\partial x$. Substituting the modified velocity equation into Eq. (9.1) and using the definition $Q = VA$, we obtain

$$\frac{\partial A}{\partial t}+\frac{\partial VA}{\partial x}=S^a+S^r-S^e-S^g+S^{o1}+S^{o2} \tag{9.15}$$

It is noted that Eq. (9.15) represents the advective transport of the cross-sectional area, A [L^2]. It is a linear advective transport equation, an ideal equation amenable for numerically innovative advective transport algorithm. To achieve transient simulations, either water depth or stage must be given as the initial condition. In addition, appropriate boundary conditions need to be specified to match the corresponding physical configuration. In a kinematic wave approach, boundary conditions are required only at upstream boundaries. An upstream boundary point can be an open boundary or a closed boundary. On an open upstream boundary, either the cross-sectional area (equivalent to water depth or water stage) or the flow rate can be specified. The flow rate through a closed upstream boundary point is by default equal to zero.

4. Thermal Transport Equation

The thermal transport equation is derived based on the conservation principle of energy:

$$\begin{aligned}\frac{\partial(\rho CAT)}{\partial t}+\frac{\partial(\rho CQT)}{\partial x}-\frac{\partial}{\partial x}\left(D^hA\frac{\partial T}{\partial x}\right)&=S_h^a+S_h^r+S_h^n-S_h^b\\&-S_h^e-S_h^s+S_h^g+S_h^{o1}+S_h^{o2}+S_h^c\end{aligned} \tag{9.16}$$

where ρ is the water density [M/L^3]; C is the heat capacity of water [$L^2/t^2/T$]; T is the temperature [T]; D^h is the apparent thermal conductivity including the effect of dispersion, diffusion, and conduction [E/L/t/T = $ML/t^3/T$, where E is the unit of energy]; S_h^a is the heat source due to artificial injection/withdraw [E/t/L=$ML^2/t^3/L$]; S_h^r is the heat source due to rainfall [E/t/L=$ML^2/t^3/L$]; S_h^n is the heat source due to net radiation [E/t/L=$ML^2/t^3/L$]; S_h^b is the heat sink due to back radiation from water surface to the atmosphere [E/t/L=$ML^2/t^3/L$]; S_h^e is the heat sink due to evaporation [E/t/L=$ML^2/t^3/L$]; S_h^s is the heat sink due to sensible heat flux [E/t/L=$ML^2/t^3/L$]; S_h^g is the heat source due to exfiltration from subsurface [E/t/L=$ML^2/t^3/L$]; S_h^{o1} is the heat source from overland flow via bank 1 [E/t/L=$ML^2/t^3/L$]; S_h^{o2} is the heat source from overland flow via bank 2 [E/t/L=$ML^2/t^3/L$]; and S_h^c is the heat source due to chemical reaction [E/t/L=$ML^2/t^3/L$].

To describe thermal transport, in addition to the initial conditions, boundary conditions must be specified for the temperature. Four types of global boundary conditions are provided here. The first type is the Dirichlet boundary condition where the temperature is prescribed as a function of time. The second type is the variable boundary condition where the temperature gradient is zero if the flow is directed out of the system. If the flow is directed into the system, the energy-flow rate is given by the product of the time-dependent incoming-fluid specific energy and the water-flow rate. The third type is the Cauchy boundary condition where the energy-flow rate is prescribed as a function of time. The fourth type is the Neumann boundary condition where the energy-flow rate due to the temperature gradient is prescribed as a function of time.

Two internal boundary conditions must be specified: one for the junction and the other for control structures. At any junction, the principle of energy balance and the formulation of energy fluxes from joining reaches to the junction are used to yield the governing boundary equations. At any control structure, the continuity of energy fluxes and the formulation of energy fluxes across the structure form the basis to yield the boundary equation [9].

5. Salinity Transport Equation

The salinity transport equation is derived based on the conservation principle of salt:

$$\frac{\partial(AS)}{\partial t}+\frac{\partial(QS)}{\partial x}-\frac{\partial}{\partial x}\left(D^{s}A\frac{\partial S}{\partial x}\right)=M_{s}^{a}+M_{s}^{r}+M_{s}^{g}+M_{s}^{ol}+M_{s}^{o2} \qquad (9.17)$$

where S is the salinity [M/L^3]; D^s is the longitudinal dispersion coefficient for salinity [L^2/t]; M_s^a is the artificial source of the salt [M/t/L]; M_s^r is the salt source from rainfall [M/t/L]; M_s^g is the salt source from subsurface [M/t/L]; M_s^{o1} is the salt source from overland via river bank 1 [M/t/L]; and M_s^{o2} is the salt source from overland source via river bank 2 [M/t/L]. Four types of global boundary conditions and two types of internal boundary conditions are similar to those for thermal transport with "salt-flow rates" replacing "energy-flow rates" and salinity replacing "temperature."

6. Sediment Transport Equation

Both bed and suspend sediment transport processes are considered in WASH123D. The governing equations for bed sediment are derived based on the mass balance of sediments on river beds while those for suspend sediments are obtained based on the conservation principle of sediments as

$$\frac{\partial(PM_{n})}{\partial t}=P(D_{n}-R_{n}) \qquad (9.18)$$

$$\frac{\partial(AS_{n})}{\partial t}+\frac{\partial(QS_{n})}{\partial x}-\frac{\partial}{\partial x}\left(AD^{n}\frac{\partial S_{n}}{\partial x}\right)=M_{n}^{a}+(R_{n}-D_{n})P+M_{n}^{o1}+M_{n}^{o2} \qquad (9.19)$$

where P is the river/stream/canal cross-sectional wetted perimeter [L], M_n is wetted perimeter-averaged concentration of the n-th bed sediment in mass per unit bed area [M/L^2], D_n is the deposition rate of the n-th sediment in mass per unit bed area per unit time [M/L^2/T], R_n is the erosion rate of the n-th sediment in mass per unit bed area per

unit time [M/L^2/T], S_n is the cross-sectionally-averaged concentration of the n-th suspend sediment in the unit of mass per unit media volume [M/L^3], D^n is the longitudinal dispersion coefficient [L^2/T] for the n-th fraction of suspend sediment, M_n^a is the artificial source of the n-th suspend sediment [M/t/L], and M_n^{o1} and M_n^{o2} are overland sources of the n-th suspend sediment from river banks 1 and 2, respectively [M/t/L]. To complete the mathematical description of sediment transport, initial conditions for every bed sediment fractions must be given and both initial and boundary conditions for every suspend sediment fractions must be prescribed. The initial conditions can either be obtained from the simulation of steady-state version of Eq. (9.18) and Eq. (9.19) or from field measurements. The same four types of global boundary conditions and two types of internal boundary conditions described for salinity transport are included for each suspend sediment fraction.

7. Biogeochemical Transport Equation

From a mathematical point of view, the temporal-spatial distribution of the M biogeochemical species in a river/stream/canal system is described with a set of reactive transport equations as

$$\frac{\partial A\rho_i C_i}{\partial t} + \alpha_i L(\rho_i C_i) = M_i^a + M_i^r + M_i^g + M_i^{o1} + M_i^{o2} + Ar_i\big|_N$$
$$\text{where } L(C_i) = \frac{\partial Q\rho_i C_i}{\partial x} - \frac{\partial}{\partial x}\left(AD^c \frac{\partial \rho_i C_i}{\partial x}\right) \tag{9.20}$$

Where ρ_i is the density of the phase associated with species i [M/L^3]; C_i is the concentration of the i-th species in mass per unit phased mass [M/M]; t is the time [t]; α_i is 0 for immobile species and 1 for mobile species; L is the advection-dispersion/diffusion transport operator; M_i^a, M_i^r, M_i^g, M_i^{o1}, M_i^{o2} are the source of the i-th species due to artificial injection, rainfall, groundwater, over land input through river banks 1 and 2 in mass rate per unit x-length [M/t/L]; $r_i|_N$ is the production rate of the i-th species due to N biogeochemical reactions in mass rate per unit medium volume [M/t/L^3]; V is the velocity [L/t]; and D^C is the hydrodynamic dispersion coefficient for chemical species [L^2/t]. The determination of $r_i|_N$ is a primary challenge in water quality modeling. Instead of using an *ad hoc* method to formulate $r_i|_N$, we use reaction-based formulations. In a reaction-based formulation, $r_i|_N$ is given by the summation of rates of all reactions in which the i-th species participates,

$$r_i\big|_N = \frac{d\rho_i C_i}{dt}\Big|_{reaction} = \sum_{k\in N}(\nu_{ik} - \mu_{ik})R_k,\ i \in M \tag{9.21}$$

where ν_{ik} is the reaction stoichiometry of the i-th species in the k-th reaction associated with the products, μ_{ik} is the reaction stoichiometry of the i-th species in the k-th reaction associated with the reactants, and R_k is the rate of the k-th reaction. Substituting Eq. (9.21) into Eq. (9.20) results in transport equations of M species as

$$\frac{\partial A\rho_i C_i}{\partial t} + \alpha_i L(\rho_i C_i) =$$
$$M_i^a + M_i^r + M_i^g + M_i^{o1} + M_i^{o2} + A\sum_{k\in N}(\nu_{ik} - \mu_{ik})R_k,\ i \in M \tag{9.22}$$

Equation (9.21) governs the dynamics of immobile species while Equation (9.22) governs the transport of mobile species subject to biogeochemical reaction processes. Either a primitive approach or a diagonalization approach can be employed to integrate Eq. (9.22) to give spatial-temporal distributions. In a primitive approach, after reaction networks are hypothesized and their reaction rates are formulated, they are substituted into Eq. (9.22) to form a set of transport equations, which are then integrated to yield the distributions and evolutions of water quality in a region of interest. When some of the reaction rates are infinite, i.e., some fast equilibrium reactions taking place in the system, this approach is not adequate [12]. Here, we will take a diagonalization approach, in which Eq. (9.22) is reduced to three subsets of equations with the Gauss-Jordan decomposition of the reaction matrix (ν_{ik} -μ_{ik})

$$R_k = \infty \ \Rightarrow\ K_k^{\ e} = \prod_{i=1}^{M}(A_i)^{\nu_{ik}} \Big/ \prod_{i=1}^{M}(A_i)^{\mu_{ik}},\ k \in N_E \tag{9.23}$$

$$\frac{\partial AE_i}{\partial t} + L(E_i^m) =$$
$$E_i^a + E_i^r + E_i^g + E_i^{o1} + E_i^{o2} + A\left(D_{ik}R_k + \sum_{j\in N_{KD(k)}} D_{ij}R_j\right),\ k \in N_{KI},\ i \in M \tag{9.24}$$

$$\frac{\partial AT_j}{\partial t} + L(T_j^m) = T_j^a + T_j^r + T_j^g + T_j^{o1} + T_j^{o2},\ j \in N_C,\ i \in M \tag{9.25}$$

where $K_k^{\ e}$ is the equilibrium constant of the *k*-th fast reaction; A_i is the activity of the *i*-th species; N_E is the number of equilibrium reactions; E_i and E_i^m are the concentration of the *i*-th kinetic variable and its mobile composition, respectively, resulting from the decomposition of the reaction matrix; E_i^a, E_i^r, E_i^g, E_i^{o1}, and E_i^{o2} are the source of the *i*-th kinetic variable from artificial addition, rainfall, groundwater exfiltration, overland bank 1, and overland bank 2, respectively; D_{ij} is the *i*-th row and *j*-th column of the decomposed reaction matrix; $N_{KD(k)}$ is the subset of linearly dependent kinetic reactions which depends on the *k*-th linearly independent reaction; N_{KI} is the number of linearly independent slow kinetic reactions; T_j and T_j^m are the concentration of the *j*-th component and its mobile composition, respectively, resulting from the decomposition of the reaction matrix; T_j^a, T_j^r, T_j^g, T_j^{o1}, and T_j^{o2} are the source of the *j*-th component from artificial addition, rainfall, groundwater exfiltration, overland bank 1, and overland bank 2, respectively; and N_C is the number of components. Equations (9.23) through (9.25) along with initial and boundary conditions form the basis of a computational model. For every mobile species, the same four types of global boundary conditions and two types of internal boundary conditions specified for salinity transport are included. From the boundary conditions for biogeochemical species, the boundary conditions for kinetic variables and components can be derived.

B. Two-Dimensional Overland Flow Regime.

The governing equations for two-dimensional density-dependent overland flow and reactive biogeochemical transport over the land surface can be derived based on the conservation principle of mass, energy, and momentum just as in the case of one-dimensional rive/stream/canal networks. These governing equations, which correspond to Eq. (9.1) and (9.2), (9.8) through (9.10), (9.15), (9.16), (9.17), (9.18) and (9.19), and (9.23) through (9.25), can be obtained without a laborious derivation, i.e., they can simply be had based on one-dimensional equations. This is achieved by (1) replacing the cross-sectional area A with the water depth h, (2) replacing the top width B with *1* (one), (3) replacing the wet perimeter P with *1* (one), (4) replacing the hydraulic radius R with *1* (one), (5) replacing the discharge Q with $\mathbf{V}h$ (where $\mathbf{V}$ is the depth-averaged velocity vector), and (6) replacing the partial differential operator $\partial()/\partial x$ with the divergence operator $\nabla_{xy}\cdot()$ if it operates on a vector or with the gradient operator $\nabla_{xy}()$ if it operates on a scalar [The subscript xy is meant to operate over the x and y coordinates]. In addition, all source terms in the one-dimensional equations, which are due to the contribution of overland, should be dropped in their corresponding two-dimensional equations. Three characteristic equations of the fully dynamic wave approach in modeling two-dimensional sheet flow can be derived in a manner similar to the case of one-dimensional river flow [9].

All types of global boundary conditions that are included in the one-dimensional cases are included in the two-dimensional cases. The internal boundary conditions of control structures (mainly culverts) are also included. The internal boundary conditions of junctions are not needed in the case of two-dimensional problems. However, a new type of internal boundary conditions on the interface between the overland regime and river/stream/canal networks is implemented. This is done (1) by settling two-dimensional fluxes equal to one-dimensional source terms and (2) imposing the equality of water surfaces across the interface between the overland regime and the river when they are continuous or by formulating the fluxes when they are not [9].

C. Three-Dimensional Subsurface Media.

1. Density-Dependent Flow

The governing equation of subsurface density dependent flow through saturated-unsaturated porous media can be derived based on the conservation law of water mass [13]. It is written as follows

$$\begin{aligned} &\frac{\rho}{\rho_o} F \frac{\partial h}{\partial t} = -\nabla\cdot\left(\frac{\rho}{\rho_o}\mathbf{V}\right) + \frac{\rho^*}{\rho_o} q, \\ &\mathbf{V} = -\mathbf{K}\cdot\left(\frac{\rho_o}{\rho}\nabla h + \nabla z\right), \quad F = a'\frac{\theta_e}{n_e} + \beta'\theta_e + n_e\frac{dS}{dh} \end{aligned} \tag{9.26}$$

where ρ is the density of water [M/L^3]; ρ_o is the reference density of water [M/L^3]; F is the water capacity [1/L]; h is the referenced pressure head [L]; ρ^* is the density of source

water; q is the source and/or sink [$L^3/t/L^3$]; **V** is the Darcy velocity [L/t]; **K** is the hydraulic conductivity tensor [L/t]; z is the potential head [L]; α' and β' are the modified compressibility of the medium and water [1/L]; θ_e is the effective moisture content [L^3/L^3]; n_e is the effectively porosity [L^3/L^3]; and S is the degree of saturation.

Five types of boundary conditions are taken into account. The first type is the Dirichlet boundary condition where the pressure head is prescribed as a function of time. The second type is the Cauchy boundary condition where the volumetric fluxes are prescribed as functions of time. The third type is the Neumann boundary condition where the pressure-gradient fluxes are prescribed as functions of time. The fourth type is the radiation boundary condition where the volumetric fluxes are proportional to the difference between the pressure head and river depth. The fifth type is the variable boundary conditions where either a Dirichlet boundary condition or a flux boundary condition is chosen by the model using a cyclic iteration approach. The fourth type boundary condition is used only when the subsurface flow is not coupled to the river flow and the fifth type of boundary condition is used only when the subsurface flow is not coupled to the overland flow.

2. Thermal Transport

The thermal transport equation is derived based on the conservation of energy:

$$\frac{\partial\left[\left(\rho C\theta+\rho_b C_m\right)T\right]}{\partial t}+\nabla\cdot\left(\rho C\mathbf{V}T\right)-\nabla\cdot\left(\mathbf{D^h}\cdot\nabla T\right)=H^a+H^c \qquad (9.27)$$

where θ is the moisture content [L^3/L^3]; ρ_b is the bulk density of the media [M/L^3]; C_m is the heat capacity of the matrix [$L^2/t^2/T$]; T is the temperature [T]; $\mathbf{D^h}$ is the apparent thermal conductivity tensor including the effect of dispersion, diffusion, and conduction [E/t/L/T = $ML/t^3/T$, where E is the unit of energy]; H^a is the heat source due to artificial injection/withdraw [$E/t/L^3$ =$M/L/t^3$], and H^c is the heat source due to biogeochemical reaction [$E/t/L^3$=$M/L/t^3$].

In addition to the initial boundary condition, boundary conditions must be specified for the temperature. Five types of global boundary conditions are provided. The first type is the Dirichlet boundary condition where the temperature is prescribed as functions of time. The second type is the Cauchy boundary condition where the heat flux is prescribed as a function of time. The third type is the Neumann boundary condition where the temperature gradient is prescribed as a function of time. The fourth type is the variable boundary conditions where the temperature gradient is zero if the flow is directed out of the region. If the flow is directed into the region, the heat flux is given by the product of the time-dependent incoming fluid temperature and discharge.

The fifth type is the energy budget condition applied at the atmosphere-land interface

$$-\mathbf{n}\cdot\left(\rho C\mathbf{V}T-\mathbf{D^h}\cdot\nabla T\right)=H_n-H_b-H_e-H_s \qquad (9.28)$$

where H_n is the heat source from net radiation [$E/t/L^2$=M/t^3]; H_b is the heat sink due to back radiation from the surface to the atmosphere [$E/t/L^2$=M/t^3]; H_e is the heat sink due to evaporation [$E/t/L^2$=M/t^3]; and H_s is the heat sink due to sensible heat flux [$E/t/L^2$=M/t^3].

Beside the five types of global boundary conditions, two interface boundary conditions may be specified: one for the exchange of energy/heat flux between the

subsurface media and river/stream/canal networks and the other for energy/heat exchange between the subsurface media and the overland regime. Detail mathematical descriptions of these two types of interfacial boundary conditions can be found elsewhere [9].

3. Salinity Transport

The salinity transport equation for three-dimensions is similar to Equation (9.17) of one-dimension,

$$\frac{\partial(\theta S)}{\partial t} + \nabla\cdot(\mathbf{V}S) - \nabla\cdot(\theta\mathbf{D}^{\mathbf{s}}\cdot\nabla S) = M_s^a \tag{9.29}$$

where S is the salinity [M/L^3]; $\mathbf{D}^{\mathbf{s}}$ is the longitudinal dispersion coefficient [L^2/t]; and M_s^a is the artificial source of the salt [M/t/L^3]. The same four types of global boundary conditions for one-dimension and two-dimensions are included in three-dimensions. In addition, two interface-boundary conditions may be specified: one for the exchange of salt flux between the subsurface media and river/stream/canal networks and the other for salt exchange between the subsurface media and the overland regime. Mathematical descriptions of these two interfacial boundary conditions can be found in Yeh et al. [9].

4. Reactive Biogeochemical Transport

Reactive biogeochemical transport equations for three-dimensions are similar to those for one-dimension and are given below [9]

$$\begin{aligned}&\frac{\partial\theta_i\rho_i C_i}{\partial t} + \alpha_i L(\rho_i C_i) = M_i^a + r_i\big|_N \\ &\text{where } L(\rho_i C_i) = \nabla\cdot(V\rho_i C_i) - \nabla\cdot\left[\theta D^c\cdot\nabla(\rho_i C_i)\right]\end{aligned} \tag{9.30}$$

$$r_i\big|_N = \frac{d\theta_i\rho_i C_i}{dt}\Big|_{reaction} = \sum_{k\in N}(\nu_{ik}-\mu_{ik})R_k,\ i\in M \tag{9.31}$$

$$\frac{\partial\theta_i\rho_i C_i}{\partial t} + \alpha_i L(\rho_i C_i) = M_i^a + \sum_{k\in N}(\nu_{ik}-\mu_{ik})R_k,\ i\in M \tag{9.32}$$

$$R_k = \infty \ \Rightarrow\ K_k^{\ e} = \prod_{i=1}^{M}(A_i)^{\nu_{ik}} \Big/ \prod_{i=1}^{M}(A_i)^{\mu_{ik}},\ k\in N_E \tag{9.33}$$

$$\frac{\partial\theta_i E_i}{\partial t} + L(E_i^m) = E_i^a + \left(D_{ik}R_k + \sum_{j\in N_{KD(k)}} D_{ij}R_j\right),\ k\in N_{KI},\ i\in M \tag{9.34}$$

$$\frac{\partial\theta_i T_j}{\partial t} + L(T_j^m) = T_j^a,\ j\in N_C,\ i\in M \tag{9.34}$$

where θ_i is the volume fraction of the phase associated with the i-th species; E_i and E_i^m are the concentration of the i-th kinetic variable and its mobile composition, respectively, resulting from the decomposition of the reaction matrix; E_i^a is the source of the i-th kinetic variable from artificial addition in mass per unit medium volume; T_j and T_j^m are the concentration of the j-th component and its mobile composition, respectively; T_j^a is the source of the j-th component from artificial addition in mass per unit medium volume.

Equations (9.33) through (9.35) along with initial and boundary conditions form the basis of a computational model for reactive transport in subsurface media. For every mobile species, the same four types of global boundary conditions for one-dimension and two-dimensions are included in three-dimensions, from which the global boundary conditions for E_i and T_j can be derived using the definition of E_i and T_j.

D. Coupling of Flow and Transport among Various Media.

One of the critical issues in a first-principle, physics-based watershed model is its treatment of coupling among various media. There appear a number of watershed models that have dealt with each component medium on the bases of first principle in the past decade (MIKE SHE [14], SHETRAN [15], MODFLOW-HMS [16], InHM [17], GISWA [18], SFRSM-HSE [19], WASH123D [9]). However, rigorous considerations on coupling among media seemed lacking. For example, a linkage term is normally formulated between the river/stream/canal dynamics and subsurface fluid flow (e.g., MODNET [20]) or between overland and subsurface flows (e.g., MIKE SHE). The linkage term usually introduces non-physics-based parameters. As a result, such watershed models have degraded even though each media-component module has taken a first-principle, physics-based approach. A rigorous treatment of coupling media should be based the continuity of mass, momentum, and state variables across media interfaces. This is the approach taken here. Mathematical statements on coupling between pairs of media are too long to cover in this Chapter. Only conceptual statements are briefly presented, detail mathematical representations to translate these statements can be found elsewhere [9].

1. Coupling between River/Stream/Canal Networks and Overland Regime

The fluxes between overland regimes and canal/stream/river network are dynamic and depend on the water surface elevations in the vicinity of the interface between the canal/stream/river and overland regime. The basic principle of coupling is to impose continuity of fluxes and the state variables (water surface elevations, temperature, and salinity, and chemical concentrations in the overland regime and in the river/stream/canal network), if these state variables do not exhibit discontinuity. If the state variables exhibit discontinuities, then linkage terms are used to simulate the volumetric fluxes and simplified equations are used to calculate the heat, salinity, sediment, and biogeochemical fluxes.

When a levee is present on the bank of canal, there are several possibilities of dynamic interactions between overland flow and canal flow dynamics. If water surfaces in both the overland regime and the canal are below the top of the levee, the two flow systems are decoupled. When the water surface in the overland regime is above the top of the levee and in the canal is below the top of the levee, the fluxes of water, heat, salt, and biogeochemical species are functions of the water depth in the overland regime. On the other hand, when the water surface in the overland regime is below the top of the levee and in the canal is above the top of the levee, the fluxes are functions of the water depth in canals. When the water surfaces in the overland and canal are above the top of the levee, then the continuity of water flux and water surface must be imposed. For

scalar transport (including thermal, salinity, and biogeochemical species), either continuity of state variables and mass fluxes may be imposed or the mass fluxes may be formulated based on the flow direction considering only the advective transport.

When a levee is not present on the bank of the river, there are two possibilities of dynamic interactions between overland flow and river flow dynamics. If water surface in the river falls below the bank, fluxes are either zero if the overland flow is not present or are nonzero and directed from the overland into the river if overland flow is present. When the water surface in the river is above the bank, the direction of flow can be either from the overland into the river or from the river into the overland depending on the flow dynamics in the overland and in the river. The water flux is obtained by imposing the continuity of the water surface. Fluxes for scalar transport can be obtained either by imposing the continuity of state variables or by formulating fluxes considering only the advective transport.

2. Coupling between Overland Regime and Subsurface Media

The volumetric flux between overland regime and subsurface media is obtained by imposing continuity of fluxes and state variables, if these state variables do not exhibit discontinuity. If the state variables exhibit discontinuity, then a linkage term is used to simulate the flux. Let us consider the interaction between the overland and subsurface flows. There are two cases: in one case, there are no impermeable layers on the ground surface and, in another case, there are thin layers of very impermeable layers such as pavements or sediment deposits on the ground surface. For the case of no impermeable layers on the ground surface, it can easily be seen that the pressures in the overland flow and in the subsurface media will be continuous across the interface. Thus, the interaction must be simulated by imposing continuity of pressures and fluxes. For the case with thin impervious layers, one can include the impervious layers as part of the subsurface media or exclude these layers from the modeling. If one includes the thin layers, then it is obvious the pressures in the overland flow and in the layer are continuous across the interface, thus continuity of pressure and flux must be imposed to simulate the interaction. On the other hand, if the thin layers are not included, it is obvious that the pressures in the overland flow and the subsurface are not continuous across the removed layers. Then a linkage-term is used to model the flux across the interface. The parameters in the linkage term are the material properties and geometry of the removed layers. These parameters, in theory, can be obtained independent of model calibration.

The coupling of scalar transport between the overland regime and subsurface media can be achieved by assuming advective transport only if the state variables are discontinuous across the interface. Otherwise, the coupling must be made by imposing the continuity of state variables across the interface to yield appropriate fluxes.

3. Coupling between Subsurface Media and River/Sream/CanalNetworks

The coupling between subsurface media and river/stream/canal/networks is almost identical to that between the subsurface media and overland regime.

III. NUMERICAL APPROXIMATIONS

One of the most critical issues in a first-principle, physics-based watershed modeling is the use of appropriate numerical methods to approximate the governing equations. For research applications, the model needs to use accurate and robust methods. For practical applications, it needs to employ efficient and robust methods. For hyperbolic-dominant transport equations such as the fully dynamic wave approach of flow and the advection-dominant scalar transport, it is well known that the semi-Largrangian (SL) method is most efficient in discretizing the advection transport while the conventional second-order finite element or finite difference methods are sufficient to approximate the diffusive/dispersive transport. Considering that there can be wide ranges of flow and transport conditions for real-world problems, we provide many numerical options in WASH123D.

For surface water flow simulations, the numerical method that is most appropriate for a particular approach is used. In kinematic-wave approaches, the semi-Lagrangian method (backward particle tracking) is used to numerically approximate the kinematic-wave equation. In the diffusive wave approach, either the Galerkin finite element method or the semi-Lagrangian method is employed to numerically solve the diffusion equation governing the transport of water surface elevation. In the fully dynamic-wave approach, the hybrid Lagrangin-Eulerian finite element method is applied to approximate the method of characteristic (MOC) form of wave equations. First, water depth and velocity are computed with the backward method of characteristics. Then the Galerkin finite element method is applied to the Lagrangin form of an eddy-diffusion equation. For subsurface flow simulations, the Galerkin finite element method is used to discretize the Richards equation. The Picard method is applied to deal with the nonlinearity of flow equations.

For transport simulations (including thermal, salinity, sediment, and water quality), two options are provided to discretize the governing sediment and biogeochemical transport equations: hybrid Lagrangian-Eulerian finite element methods or conventional finite element methods. Three schemes are employed to handle the coupling between the hydrologic transport and biogeochemical reactions: fully implicit sequential iteration approach, operator splitting, and mixed predictor-corrector and operator-splitting. The Newton-Raphson method was used to solve the set of algebraic equations and ordinary equations describing the evolution of all biogeochemical species.

Details of the aforementioned numerical methods can be found elsewhere [9].

IV. DEMONSTRAVE EXAMPLES

Five example problems are used to demonstrate the design ability and flexibility of WASH123D to solve a variety of problems. Example 1 involves one-dimensional flow problems with three cases to illustrate the capability of the model to simulate subcritical, mixed subcritical and supercritical, and hydraulic jump problems and to assess the adequacy of using diffusive and dynamic wave approaches. Example 2 is a two-dimensional overland flow problem used to compare the simulations with kinematic, diffusive, and fully dynamic wave approaches. Example 3 is a three-dimensional density

dependent subsurface flow problem. Example 4 is a flow problem in an integrated one-dimensional canal network, overland regime, and subsurface media system demonstrating the successful coupling based on physics. Example 5 is a reactive biogeochemical problem in a canal illustrating the generality of the paradigm in modeling water quality.

A. One-Dimensional River/Stream/Canal Flow Problems.

Three cases are presented for the one-dimensional problems in the river/stream/canal system. Case 1 is a steady-state subcritical flow problem, which shows there are some errors in the diffusive wave approximation even for this simple problem. Case 2 is a steady-state mixed subcritical and supercritical problem, which is designed to demonstrate the magnitude of errors introduced with the diffusive wave approximation. Case 3 is a steady-state, mixed subcritical and supercritical problem with a hydraulic jump. This problem demonstrates that the diffusive wave approximation is not adequate for this complicated problem. In all three cases, steady-state simulations were achieved via transient simulations with constant boundary and source conditions.

1. Subcritical Flow

This is the test problem published by MacDonald et al. [21], where an analytical solution for the problem is available. The channel is rectangular with a width of 10 m. The total length is 1,000 m. A constant flow of 20 m^3/s passes through. The flow is subcritical over the entire channel. A water depth of 0.748409 m is specified at the downstream outlet. The Manning's n value is 0.03. The bed slope is given by an analytical function of the water depth. Simulated steady-state profiles of water depth with diffusive wave (DIW) and fully dynamic wave (FDW) approaches are given in Figure 9.3. It is seen that the FDW approach yields excellently accurate results while the DIW approach produces some errors.

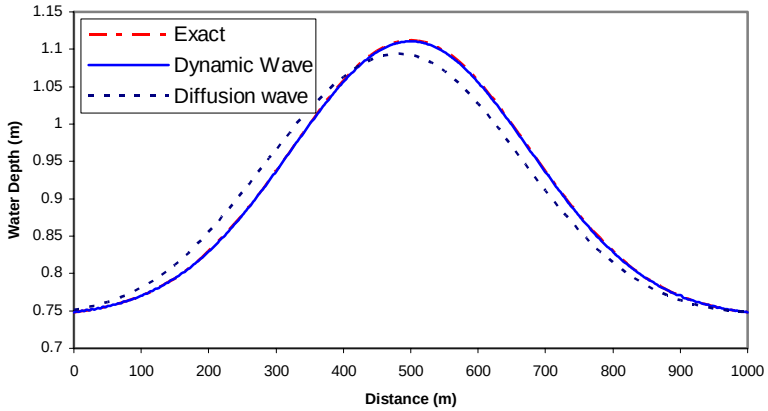

Fig. 9.3 Comparison of Simulated Water Depth Profiles with Exact Solution

2. Mixed Subcritical and Supercrical Flow

This test case was described in MacDonald et al. [21]. A 1,000 m of rectangular channel with a width of 10 m is given a constant flow rate of 20 m^3/s. The bottom slope is variable such that the flow condition at the inflow is subcritical and is supercritical at the outlet. The Manning's n value is 0.02. For the dynamic wave approach, one inflow boundary condition is specified at the upstream and no boundary condition is needed at the downstream since supercritical flows occur therein. For diffusive wave model, two boundary conditions must be given: one is the upstream boundary condition where the inflow rate is prescribed as in the case of FDW approach and the other is the downstream boundary condition. In this case, the known water depth at outlet is specified as the Dirichlet boundary conditions.

The dynamic wave model is able to solve this mixed flow problem with good accuracy (Fig. 9-4). No numerical instabilities have been encountered. The diffusive wave model also provides satisfactory results (4% error in water depth). The Froude number profile plot not shown here confirms the mixed flow condition. It is interesting to note that the DIW model requires more input data than the FDW model, yet yields poorer simulations.

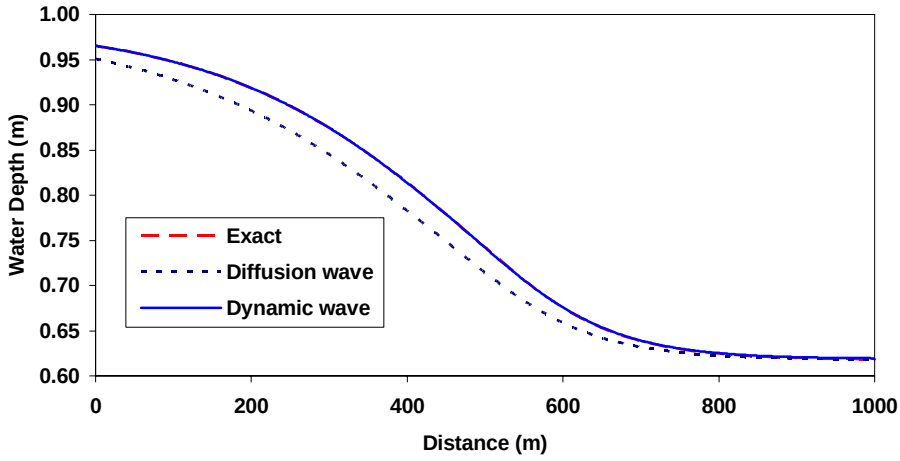

Fig. 9.4 Comparison of Simulated Water Depth Profile with Exact Solutions

3. Mixed Subcritical and Supercrical Flow with Hydraulic Jump

This test case was described in MacDonald et al. [21]. The channel is trapezoidal with a total length of 1,000 m. The upstream inflow is a constant discharge of 20 m^3/s. At the downstream outlet, a specified water depth of 1.349963 m is applied. The side slope of the trapezoidal cross-section is 1:1. The Manning's n value is 0.02. There is an abrupt change in the bed slope at x = 500 m, causing a hydraulic jump. The bottom elevation and bed slope were given in MacDonald et al. [21]. Both inflow and outflow

boundaries are subcritical. This is a non-trivial problem with source terms (roughness and bed slope) and is more realistic in testing the performance of the FEM based method of characteristics.

As expected, the accuracy of the diffusive wave approximation for this mixed flow case is not satisfactory. The error induced by diffusive wave approximation is high at the supercritical zone (Fig. 9.5).

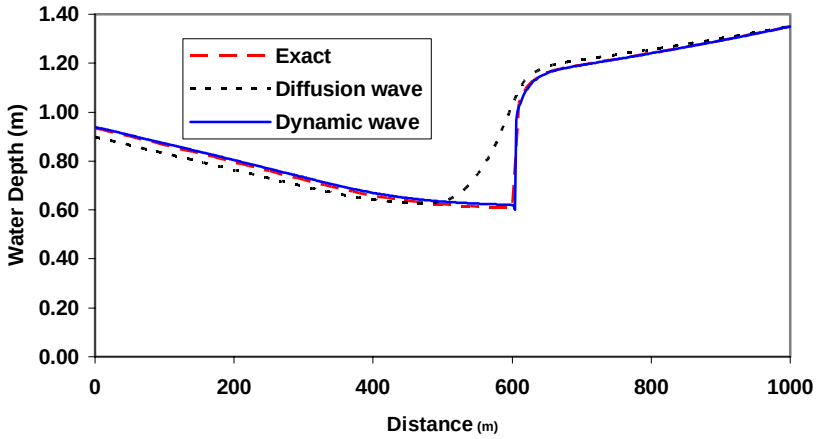

Fig. 9.5 Comparison of Simulated Water Depth Profile with Exact Solution

B. Two-Dimensional Overland Flow Problems.

A rainfall-runoff process on an impervious curved surface is simulated (Fig. 9.6). The domain is 150 m x 40 m. The bottom elevation ranges from 0.11 m to 0.31 m over a horizontal length of 150 m. The overland domain is divided into 80 elements and 105 nodes. A specified water depth of 0.1 m is applied to the downstream end boundary. All other sides are assumed to be no-flow boundaries. A Manning's n value of 0.02 is used. The rainfall intensity is 3.0^{-5} m/s for 1,800 seconds (30 minutes). The purpose of this numerical experiment is to compare the simulation results obtained with different computational methods for 2-D overland flow and validate the numerical implementation for dynamic, diffusive and kinematic wave models. The average bottom slope is 0.00133.

The fully dynamic wave equations and diffusive wave and kinematic wave approximations were applied to this problem. The simulation results were compared. The computed water levels at Node 28 (x = 20 m, y = 30 m, Z_o = 0.152 m) were compared (Fig. 9.7). This location is close to the downstream end. The maximum value of water level, found to be 0.173 m, 0.180 m and 0.181 m, was obtained with fully dynamic wave (MOC), diffusive wave (SL), and kinematic wave (SL) approaches. The difference between the dynamic wave and diffusive wave models is about 6%. This may indicate the diffusive wave approximation is not accurate for this problem. Similar conclusions can be made for the kinematic wave model. Water levels at Node 88 (x = 20 m, y = 130 m and z_o = 0.278 m), which represent the flow at upper part of the surface, were compared (Fig. 9.8). The maximum water depth at this site is 0.01124 m, 0.0094 m

and 0.00776 m for FDW (MOC), DIW (SL), and KIW (SL), respectively. The differences between the fully dynamic wave and diffusive/kinematic wave models at the upstream nodes are smaller than those at the downstream nodes as expected.

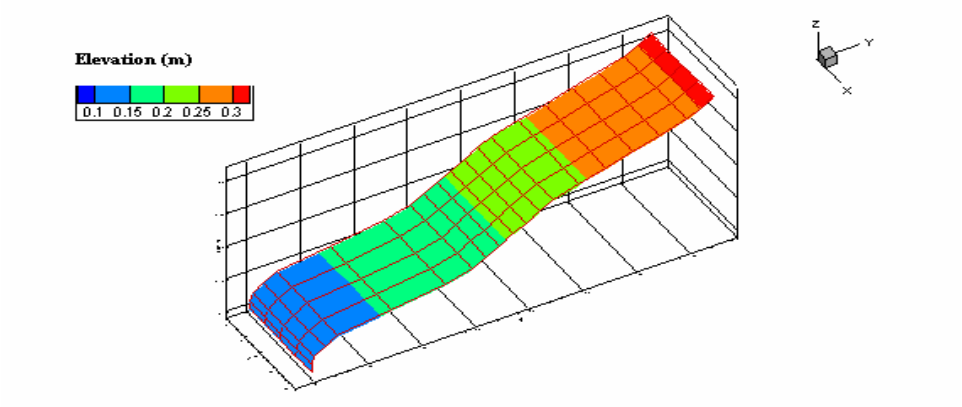

Fig. 9.6 Topography of the Land Surface

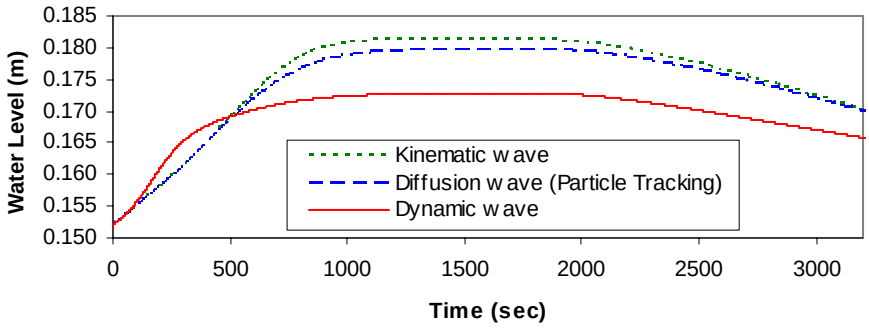

Fig. 9.7 Comparison of Simulated Water Levels

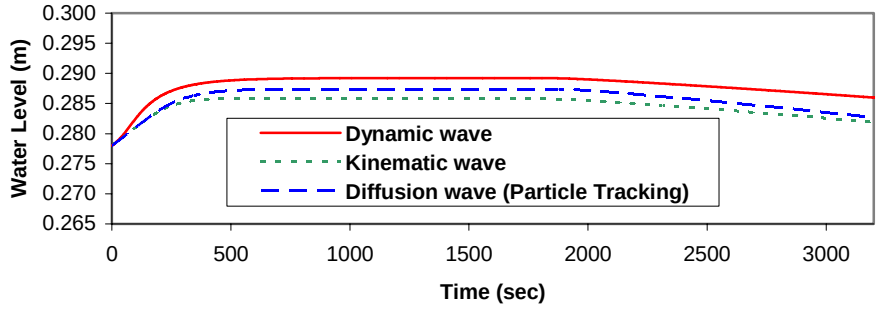

Fig. 9.8 Comparison of Simulated Water Levels

C. Three-Dimensional Density Dependent Flow in Subsurface Media.

Aquifer Storage Recovery (ASR) injects surface water into an aquifer and then recovers it for later water use. The simple case of a single ASR well is simulated. Some data refers to the 1989 ASR pilot project at Lake Okeechobee, Florida [22], but overall it is for demonstration purposes only. Three-dimensional density driven flow and transport are simulated. The injected freshwater is stored and mixed with the brackish water in the aquifer. The diameter of the ASR well is 24 inches. The screened area is located at 1300 ft to 1600 ft below land surface. The storage zone is in the artesian aquifers with a confining layer of 400 ft over it. The saturated hydraulic conductivity is 177.6 ft/day. The effective porosity is 0.25. Only the storage zone will be simulated. The thickness of the aquifer is 300 ft. A rectangular area of 1,600 x 1,600 ft is chosen for the modeling domain. The boundary is to be set away from the ASR well, so that injected water is stored within the domain. Specified head boundary conditions are assigned in the direction of natural groundwater flow to represent the background groundwater flow. Variable boundary conditions are specified at the perimeter of the ASR well. The boundary condition at the screen of the ASR well can be specified head or flux depending on the injection pumping pressure. The 3-D finite element mesh contains three layers. The total number of subsurface nodes is 3,280 and the total number of elements is 4,674. The size of the elements is designed to be finest within the vicinity of the well (Fig. 9. 9).

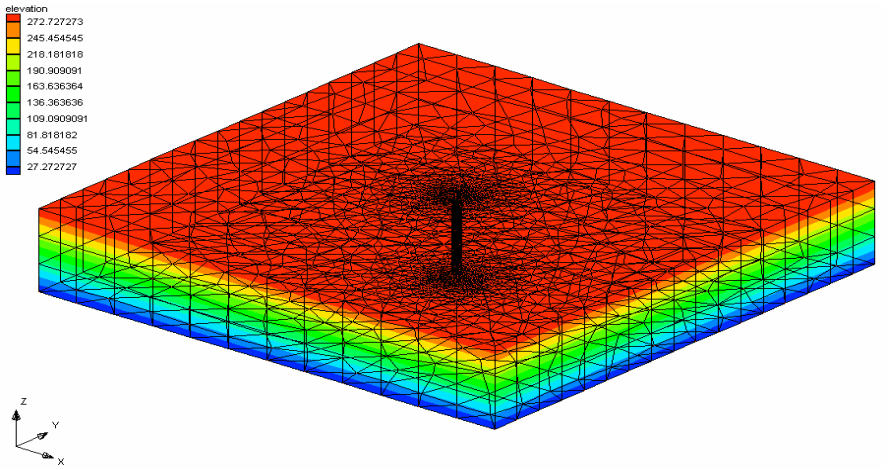

Fig. 9.9 Finite Element Discretization for the ASR Problem

The injection/recovery processes were simulated for 720 hours. The injection stopped at time = 360 hours and then recovery started until the end of the simulation. The total head and saline concentration distributions at different times were plotted (Fig. 9.10 and Fig. 9.11). The spatial distributions of total head and concentration demonstrated the impacts of background flow and density effect.

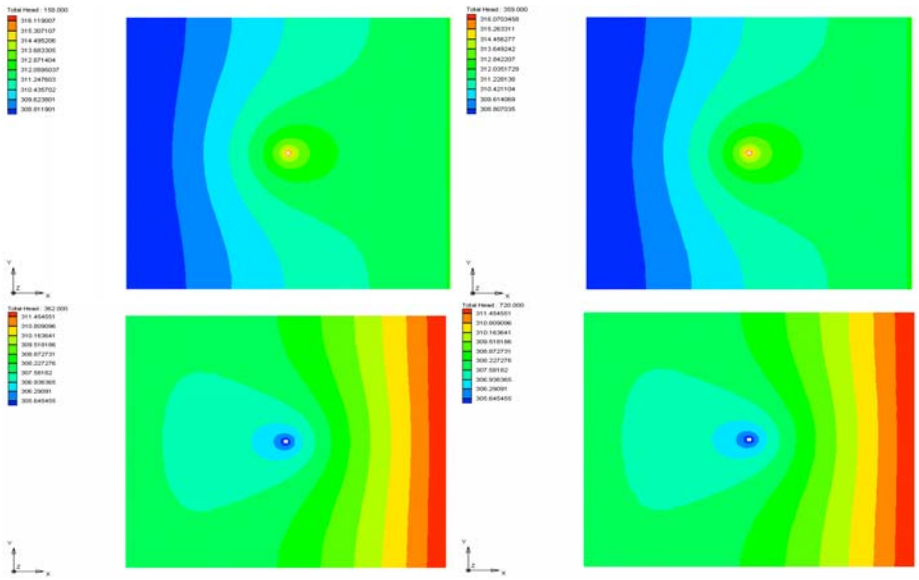

Fig. 9.10 Total Head Distribution (t = 2 [upper left], 359 [upper right], 362 [lower left] and 720[lower right] hours)

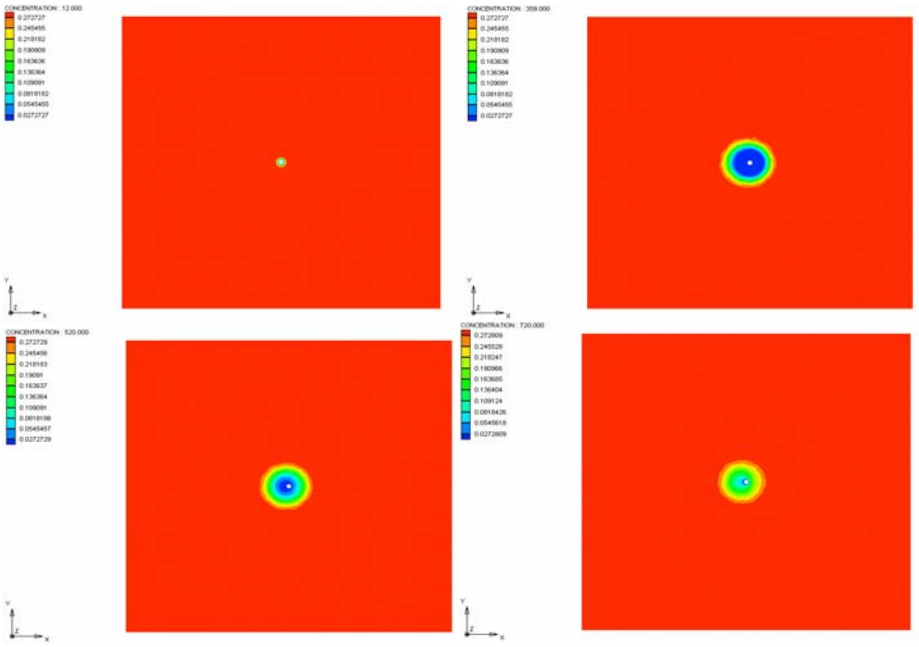

Fig. 9.11 Concentration Distribution (t = 12 [upper left], 359 [upper right], 520 [lower left] , and 720 [lower right] hours)

The total heads reach steady-state quickly, within two hours of beginning the injection and within two hours of starting the recovery (Fig. 9.10). This is due to the fact that the storativity of media for water under saturation flow conditions is from the compressibility of water and the compressibility of matrix, which are very small. Had these compressibilities been set to zero, the steady-state simulations would have been achieved instantaneously at the starts of injection and recovery. Since the storativity of the media for chemicals is the porosity, the variation of salinity is gradual with time (Fig. 9.11).

D. Coupled Canal, Overland, and Subsurface Flow.

This is a sub-regional scale modeling effort for the south Florida wetlands. The Dade model domain extends from four miles west of the L-67 Extension dike to the western shore of Biscayne bay and from one mile north of the Tamiami canal south to Florida bay. Horizontally, it covers an area of approximately of 1,200 mi^2. Vertically, it extends from the land surface to the bottom of the surficial aquifer.

Some characteristics of this model are strong interaction of overland flow, groundwater flow, and canal flow in south Florida; and complex hydraulic structure operations. The 3-D finite element mesh for subsurface media (Fig. 9.12) is complex: there are 37,760 global nodes and 65,429 elements. There are 7 layers in the vertical direction and levees are incorporated as part of the subsurface media.

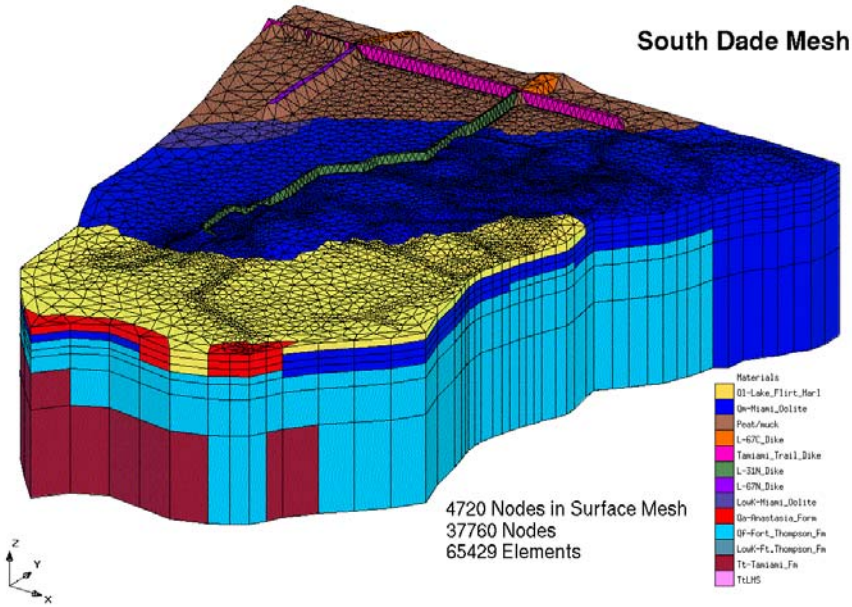

Fig. 9.12 Subsurface Finite Element Mesh

The boundary conditions for subsurface flow were determined from the SFWMM 2 x 2 model output for the northern boundary and from structure operation records for the other sides of the boundaries.

The surface water flows (2-D overland and 1-D canal flows) were simulated with the diffusion wave approach using the Galerkin finite element method. The 2-D overland flow domain consists of 4,720 nodes and 9,347 triangular elements. Levees are included in the computation domain (Fig. 9.13). Boundary conditions were determined from structure operation records along the boundary. The canal network as simplified in this simulation includes: 560 canal nodes, 506 canal elements, 55 river reaches, 20 canal junctions, and 11 interior gates (Fig. 9.13). The upstream is specified a flux boundary, providing the inflow into the canal network. The downstream are specified stage boundaries, which are given by the structure operation at downstream ends.

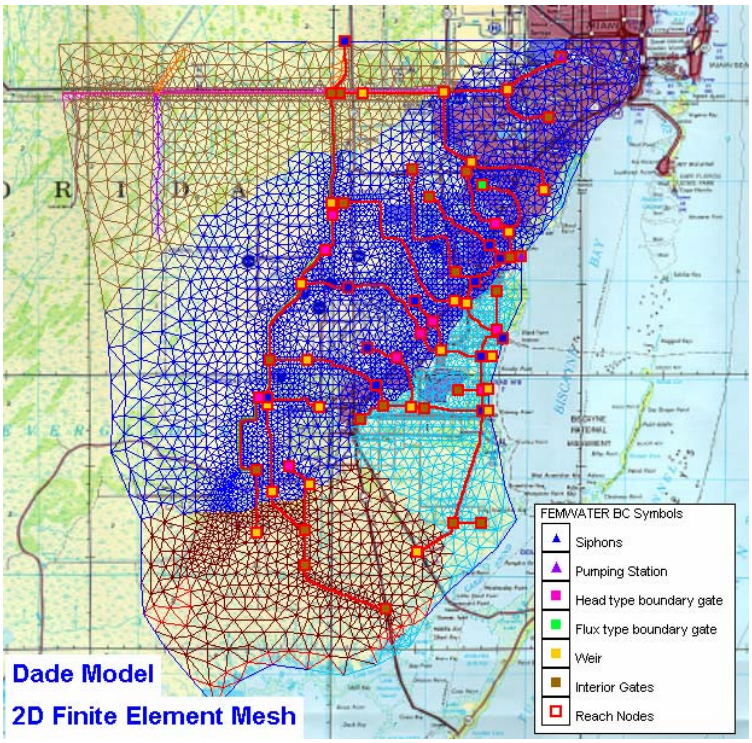

Fig. 9.13 2D Overland Mesh and 1D Canal Network

The 1D/2D/3D coupled flow simulation was first begun with a steady state of subsurface flow. Then the steady state condition was used as the initial condition of the transient flow simulation of the coupled system. Figures 9.14 and 9.15 show the simulation results of a model run. Since the levee and dike are included as part of the subsurface media, it is demonstrated that the ground water flow from the northern boundary can bypass the

less permeable levees via their underlying permeable media. It is also obvious that the canals recharge the ground water.

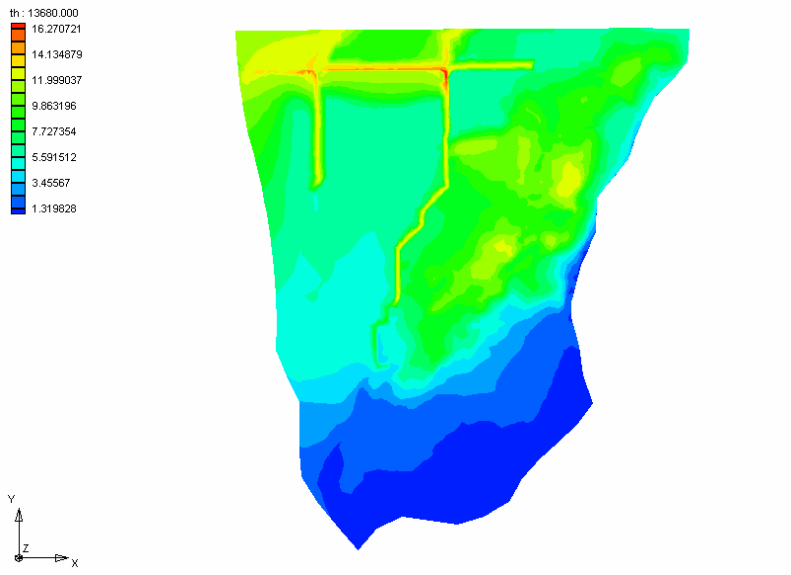

Fig. 9.14 Total head Distribution (feet) (time = 13,680 minutes = 9.5 days)

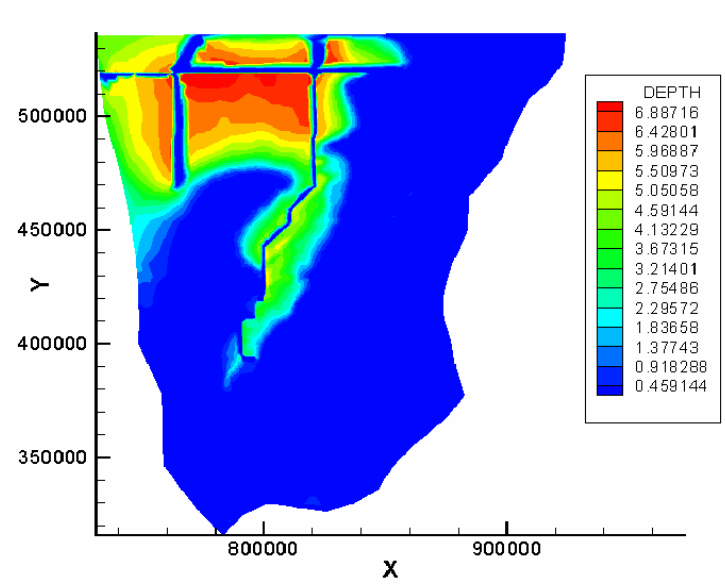

Fig. 9.15 Overland Water Depth (feet) (time = 7000 minutes = 4.9 days)

E. One-Dimensional River/Stream/Canal Water Quality Transport Problems.

To demonstrate the flexibility and generality of the paradigm to model water quality employed in WASH123D [9], the eutrophication models in QUAL2E [23], WASP5 [24], and CE-QUAL-ICM [25] can be recast in the mode of reaction networks. From the networks, the number of water quality and the number of biogeochemical reactions vary with these three widely used models. Table 1 lists the comparison of the three models via a reaction point of view. In the original reports, there are 9, 16, and 41 water qualities simulated in QUAL2E, WASP5, and CE-QUAL-ICM, respectively. In the context of reaction network, there should be 19, 27, and 66 constituents involved in QUAL2E, WASP5, and CE-QUAL, respectively. The differences between the original reports and reaction-based approaches are reconciled in the following two paragraphs.

In the case of QUAL2E, all rate equations depend on only the first 9 constituents, thus, the other 10 constituents can be decoupled from the first 9 in any simulation. Had evidence indicated that the rate of the 16 kinetic reactions also depends on the other 10 constituents in a system, then all 19 constituents should have been modeled simultaneously. Therefore, when QUAL2E is applied to any system, the first order of business is to check if the rate formulation for the 16 kinetic reactions is valid. If it is, then one can consider other issues involved in applying the model to his/her system. If any of the 16 rate equations is invalid, then one should not apply the model to his/her system.

In the case of WASP5, the issue is more complicated. First, rates of the 32 kinetic reactions as given in WASP5 were assumed not to be affected by the last five constituents. Thus, these five constituents can be decoupled from the other 22. Thus, one only needs to simulate 22 constituents simultaneously from the reaction point of view. The question is then why WASP5 only considered 16 water quality state-variables. Examination of 6 fast equilibrium reactions would reveal that the adsorption reactions of aqueous CH_2O, $CH_2O_{(b)}$, ON, $ON_{(b)}$, OP, and $OP_{(b)}$ onto sediments were formulated with a simple partition. Furthermore, rate equations are only functions of the aqueous fractions of CH_2Ot, $CH_2Ot_{(b)}$, ONt, $ONt_{(b)}$, OPt, and $OPt_{(b)}$, not functions of 12 individual species. Thus, if we eliminate these twelve species using the 6 partition equations and 6 equations defining the total, the reaction-based approach would yield 16 identical equations as those in the WASP5 report. In our reaction-based approach, we prefer to model all 22 species. This allows us, if necessary, the flexibility of more mechanistically modeling the sorption reactions and formulating the rate equations as functions of all individual species. Similarly, for CE-QUAL-ICM, we prefer to model 48 species out of the total 66 species, rather than 41 constituents. This reaction-based approach alleviates the need of modeling 7 sorption reactions with a simple partition as done in WASP5. In the decomposition of the reaction-matrix, the elimination of 7 fast equilibrium reactions is performed automatically rather then manually. Ideally, one should model all of the 66 species if some of the reaction rates are affected by the other 18 species.

Table 1. QUAL2E, WASP5, and CE-QUAL-ICM from a Reaction Point of View.

Model	QUAL2E	WASP5	CE-QUAL-ICM
Number and types of reaction	**16 kinetic and 0 equilibrium reactions:** Algal kinetics: 4 Dissolved Oxygen Balance: 4 Nitrogen Cycle: 5 Phosphorus Cycle: 3	**32 kinetic and 6 equilibrium reactions:** Phytoplankton Kinetics: 11 Dissolved Oxygen Balance: 9 Nitrogen Cycle: 11 Phosphorus Cycle: 7	**83 kinetic and 7 equilibrium reactions:** Plant and bacterial Kinetics: 14 Dissolved Oxygen Balance: 16 Nitrogen Cycle: 20 Phosphorus Cycle: 21 Silica Cycle: 16 Metal Cycle: 3
No. of species in the report	**9** O, L, Chla, N_4, N_1, N_2, N_3, P_1, and P_2.	**16** NH_3, $NH_{3(b)}$, NO_3, $NO_{3(b)}$, OPO_4, $OPO_{4(b)}$, PHYT, $PHYT_{(b)}$, CH_2Ot, $CH_2Ot_{(b)}$, O_2, $O2_{(b)}$, ONt, $ONt_{(b)}$, OPt, and $OPt_{(b)}$.	**41** Bc, Bd, Bg, DOC, LPOC, RPOC, NH_4, NO_3, DON, LPON, RPON, PO_4t, DOP, LPOP, RPOP, COD, DO, SU, SA, TAM, $POC_{1(b)}$, $POC_{2(b)}$, $POC_{3(b)}$, $NH_{41(b)}$, $NH_{42(b)}$, $NO_{31(b)}$, $NO_{32(b)}$, $PON_{1(b)}$, $PON_{2(b)}$, $PON_{3(b)}$, $PO_{41(b)}$, $PO_{42(b)}$, $POP_{1(b)}$, $POP_{2(b)}$, $POP_{3(b)}$, $COD_{1(b)}$, $COD_{2(b)}$. $SU_{1(b)}$, $SU_{2(b)}$, $SA_{1(b)}$, and $SA_{2(b)}$
No. of water quality from the reaction point of view	**19 (9 modeled)** O, L, Chla, N_4, N_1, N_2, N_3, P_1, P_2, $O_{(b)}$, $L_{(b)}$, $Chla_{(b)}$, $N_{4(b)}$, $N_{(1b)}$, $P_{(1b)}$, $P_{(2b)}$, CO_2, H_2O, and $O_{2(g)}$	**27 (22 modeled)** NH_3, $NH_{3(b)}$, NO_3, $NO_{3(b)}$, OPO_4, $OPO_{4(b)}$, PHYT, $PHYT_{(b)}$, CH_2O, CH_2Op, $CH_2O_{(b)}$, $CH_2Op_{(b)}$, O_2, $O_{2(b)}$, ON, ONp, $ON_{(b)}$, $ONp_{(b)}$, OP, OPp, $OP_{(b)}$, $OPp_{(b)}$, CO_2, H_2O, H^+, N_2, and $O_{2(g)}$.	**66 (48 modeled)** Bc, Bd, Bg, DOC, LPOC, RPOC, NH_4, NO_3, DON, LPON, RPON, PO_4d, PO_4p, DOP, LPOP, RPOP, COD, DO, SU, SAd, SAp, TAMd, TAMp, $POC_{1(b)}$, $POC_{2(b)}$, $POC_{3(b)}$, $NH_{41(b)}$, $NH_{42(b)}$, $NO_{31(b)}$, $NO_{32(b)}$, $PON_{1(b)}$, $PON_{2(b)}$, $PON_{3(b)}$, $PO_4d_{1(b)}$, $PO_4p_{1(b)}$, $PO_4d_{2(b)}$, $PO_4p_{2(b)}$, $POP_{1(b)}$, $POP_{2(b)}$, $POP_{3(b)}$, $COD_{1(b)}$, $COD_{2(b)}$, $SU_{1(b)}$, $SU_{2(b)}$, $SAd_{1(b)}$, $SAp_{1(b)}$, $SAd_{2(b)}$, $SAp_{2(b)}$, CO_2, H_2O, N_2, $O_{2(g)}$, $Bc_{(b)}$, $Bd_{(b)}$, $Bg_{(b)}$, $TAMp_{(b)}$, BPOC, BNH_4, BNO_3, BPON, BPO_4, BPOP, BCOD, BSU, BSA, and BTAM

To demonstrate the general paradigm, we apply WASP5 to a canal reach. The canal considered is 15,545 ft-long with width ranging from 15 to 40 ft. It is descretized by 9 elements with variable size of 1,690 to 1,801 ft. The flow pattern was simulated using the one-dimensional flow module of WASH123D. The calculated water depth ranges from 7.15 to 9.22 ft and river/stream velocity from 0.193 to 2.9 ft/s. Manning's roughness is 0.01. To focus on reactive biogeochemical transport, the depth of the canal bed is assumed 0.5 ft, the temperature is 15˚C, the suspended sediment concentration is $1g/m^3$, and the bed sediment concentration is 15 g/m^2 throughout the canal. Dirichlet boundary

condition is applied to the upstream boundary node. Flow-out variable boundary condition is applied to the downstream boundary node. Initial concentrations of all species and Dirichlet boundary concentrations of mobile species are listed in Table 9.2. The longitudinal dispersivity is 300 ft. A 12-day simulation is performed with a fixed time step size of 6 minutes.

Table 9.2. Chemical Species Included in the Eutrophication Simulation

Species	Notation	Initial	Boundary	Units
Ammonia Nitrogen	NH_3	0.1	1	mg N/L
Benthic Ammonia Nitrogen	$NH_{3(b)}$	0.1	-	mg N/L
Nitrate Nitrogen	NO_3	0.1	1	mg N/L
Benthic Nitrate Nitrogen	$NO_{3(b)}$	0.1	-	mg N/L
Inorganic Phosphorus	OPO_4	0.01	0.1	mg P/L
Benthic Inorganic Phosphorus	$OPO_{4(b)}$	0.01	-	mg P/L
Phytoplankton Carbon	PHYT	0.2	2	mg C/L
Benthic Phytoplankton Carbon	$PHYT_{(b)}$	0.2	-	mg C/L
Dissolved Carbonaceous BOD	CBOD	1.0	10	mg O_2/L
Particulte Carbonaceous BOD	$CBOD_{(p)}$	1.0	10	mg O_2/L
Benthic Dissolved Carbonaceous BOD	$CBOD_{(b)}$	1.0	-	mg O_2/L
Benthic Particulte Carbonaceous BOD	$CBOD_{(bp)}$	1.0	-	mg O_2/L
Dissolved Oxygen	DO	0.2	2	mg O_2/L
Benthic Dissolved Oxygen	$DO_{(b)}$	0.2	-	mg O_2/L
Dissolved Dissolved Organic Nitrogen	ON	0.2	2	mg N/L
Particulte Dissolved Organic Nitrogen	$ON_{(p)}$	0.0	0	mg N/L
Benthic Dissolved Organic Nitrogen	$ON_{(b)}$	0.2	-	mg N/L
Benthic Particulte Organic Nitrogen	$ON_{(bp)}$	0.0	-	mg N/L
Dissolved Organic Phosphorus	OP	0.035	0.35	mg P/L
Particulte Organic Phosphorus	$OP_{(p)}$	0.015	0.15	mg P/L
Benthic Dissolved Organic Phosphorus	$OP_{(b)}$	0.035	-	mg P/L
Benthic Particulte Organic Phosphorus	$OP_{(bp)}$	0.015	-	mg P/L

Figures 9.16 through 9.19 plot the concentration distribution of PHYT, DO, $PHYT_{(b)}$, and $DO_{(b)}$ at different times. The similar pattern in concentration of PHYT and DO indicates that the concentration change of these mobile species is mainly controlled by the advection-dispersion transport rather than the biogeochemical reactions (Fig. 9.16 and 9.17). However, the concentration change of immobile benthic species $PHYT_{(b)}$ and $DO_{(b)}$ is mainly affected by the biogeochemical reactions.

In the benthic immobile water phase, the concentration change of $PHYT_{(b)}$ is due to its decomposition and PHYT settling. Figure 9.18 shows increasing concentration of $PHYT_{(b)}$, indicating that the settling rate of PHYT is greater than the $PHYT_{(b)}$ decomposition rate. The concentration change of $DO_{(b)}$ is due to its consumption by oxidation and it production by diffusion from DO. Figure 9.19 shows decreasing concentration of $DO_{(b)}$ at upstream. This indicates that at the upstream the diffusion rate from DO is less than the consumption of oxidation. As the simulation time increases, there is more DO downstream. Figure 9.19 shows an increasing concentration of $DO_{(b)}$ downstream, demonstrating that the increased diffusion rate from DO is greater than the consumption by oxidation.

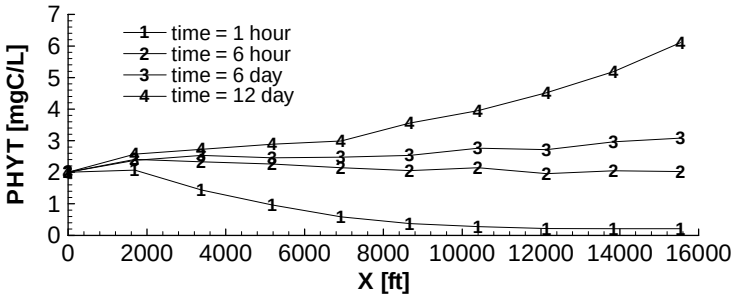

Fig. 9.16 Concentration Distribution of PHYT

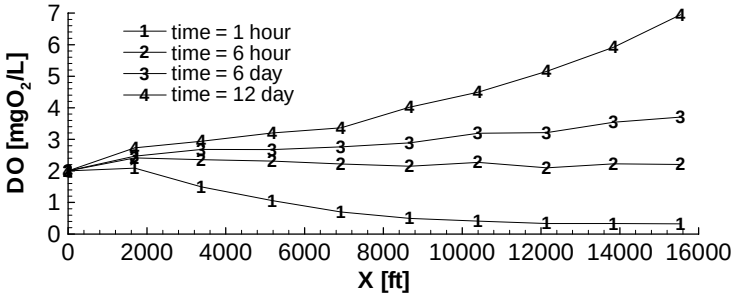

Fig. 9.17 Concentration Distribution DO

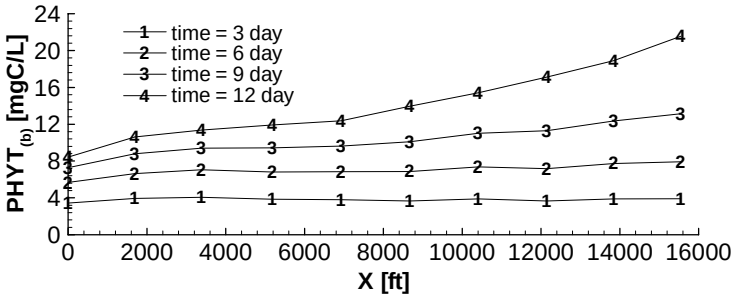

Fig. 9.18 Concentration Distribution of $PHYT_{(b)}$

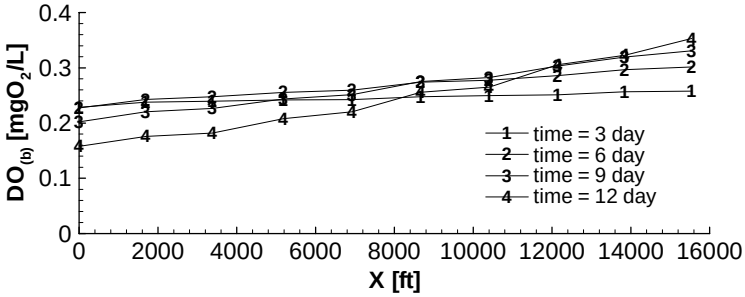

Fig. 9.19 Concentration Distribution of $DO_{(b)}$

V. SUMMARY

A first-principle, physics-based computational model has been developed that integrates multimedia of one-dimensional river/stream/canal networks, two-dimensional overland regime, and three-dimensional subsurface media and that integrates multi-processes of flows, thermal transport, salinity transport, sediment transport, and reactive biogeochemical transport in watersheds. Surface water flows in river/stream/canal networks and overland regime can be modeled with fully dynamic wave, diffusive wave, or kinematic wave options. Vadose zone and saturated zones are considered an integral system of the subsurface media in which variably saturated flows occur. Thermal and salinity transport are coupled with St Venant equations in surface waters and with Richards equations in subsurface media to provide density-dependent flow simulations. Bed sediment balance and suspend sediment transport are included to affect reactive biogeochemical transport and constitute an integral set of water quality modeling. A diagonalization approach is applied to reactive biogeochemical species transport equations to yield three subsets of governing equations that may greatly reduce the number of transport equations and that allow the formulation of reaction rate one by one.

To allow the application of the model to both research and practical problems, various numerical methods are applied to discretize the governing equations. These include characteristics-based semi-Largrangian methods for fully dynamic wave flows, finite element methods or semi-Largrangian methods for diffusive wave flows, and semi-Largrangian methods for kinematic wave flows in surface waters. For subsurface flows, the Galerkin finite element method is employed. For scalar transport (including thermal, salinity, sediment, and reactive biogeochemical transport), the hybrid Lagrangian-Eulerian method is used. Three optional schemes are implemented to deal with the interactions between transport and biogeochemical reactions.

Five example problems are used to demonstrate the design capability of the model. They also serve the purposes of need of various approaches to model surface water flows. The example of reactive biogeochemical transport shows the generality and flexibility of the diagonalized, reaction-based paradigm in modeling water quality. The three widely used water quality models can be cast in the mode of reaction networks.

ACKNOWLEDGEMENT

This research is funded by U.S.EPA-Science To Achieve Results (STAR) Program Grant #R82795602 with University of Central Florida. The work described in this chapter was authorized by Headquarters, US Army Corps of Engineers. Funding was provided by the Army Environmental Center and Civil Works projects.

VI. REFERENCES

1. Bicknell, B. R., J. C. Imhoff, J. L. Kittle, A. S. Donigian, and R. C. Johanson, 1993. Hydrolgic Simulation Program - FORTRAN (HSPF): User's Manual for Release 10.0. EPA 600/3-84-066. U.S. Environmental Protection Agency, Environmental Research Laboratory, Athens, GA

2. Huber, W. C. and R. E. Dickinson, 1988. Storm Water Management Model [SWMM] Version 4, User's Manual. EPA 600/3-88/001a. U.S. Environmental Protection Agency, Athens, GA.

3. Knisel, W. G. (ed.), 1980. CREAMS, A Field Scale Model for Chemicals, Runoff, and Erosion from Agricultural Management System. USDA Conserv. Res. Rept. No. 26, 643 pp.

4. Hydrologic Engineering Center, 1977. Storage, Treatment, Overflow, Runoff Model, STORM, User's Manual. Gnneralized Computer Program 723-S8-L7520. U.S. Army Corps of Engineers, Davis, CA.

5. Beasley, D. B. and L. F. Higgins, 1981. ANSWERS [Areal Nonpoint Sorce Watershed Environmental Response Simulation] User's Manual. EPA905/9-82-001. U.S. Environmental Protection Agency, Region 5, Chicago, IL

6. Arnold, J. G., J. R. Williams, R. H. Griggs, and N. B. Sammons, 1991. SWRRBWQ – A Basin Scale Model for Assessing Management Impacts on Water Qaulity. USDA, ARS. Grassland, Soil, and Water Research Laboratory, Temple, TX.

7. Crawford, N. H. and R. K. Linsley, 1966. Digital Simulation in Hydrology: Stanford Watershed Model IV. Technical Report No. 19, Dept. of Civil Engineering, Stanford University, Stanford, CA., 1966. 210 pp.

8. EPA, 1997. Compendium of Tools for Watershed Assessment and TMDL Development. EPA/841-B-97-006. U.S. Environmental Protection Agency, Office of Water, Washington, DC 20460.

9. Yeh, G. T., H. P. Cheng, G. B. Huang, F. Zhang, H. C. Lin, E. Edris, and D. Richards. 2004. A Numerical Model of Flow, Heat Transfer, and Salinity, Sediment, and Water Quality Transport in WAterSHed Systems of 1-D Stream-River Network, 2-D Overland Regime, and 3-D Subsurface Media (WASH123D: Version 2.0). Technical Report CHL-**-**. Waterways Experiment Station, U. S. Army Corps of Engineers, Vicksburg, MS 39180-6199.

10. Singh, V. P., 1996, Kinematic Wave Modeling in Water Resources, John Wiley & Sons, Inc.

11. Hergarten, P. S. G. and H. J. Neugebauer, 1995, An integrated model for the surface runoff and the infiltration of water, EOS, transc. Am. Geophys. Union. Vol. 76, No. 46, F320.

12. Fang, Y., G. T. Yeh, and W. D. Burgos, 2003. A Generic Paradigm to Model Reaction-Based Biogeochemical Processes in Batch Systems. Water Resources Research 33(4):1083-1118.

13. Yeh, G. T., J. R. Chang, J. P. Gwo, H. C. Lin, W. Martin, and D. Richards. 1994. 3DSALT: A Three-dimensional Salt Intrusion Model in Saturated-Unsaturated Media. Instruction Report HL-94-1. Waterway Experiment Station, U. S. Army Corps of Engineers, Vicksburg, MS.

14. Refsgaard, J. C., and B. Storm, 1995. "MIKE SHE" Computer Models of Watershed Hydrology, V. P. Singh, ed., Water Resources Publications, Littleton, Colorado, 809-846.

15. Ewen, J., G. Parkin, and P. E. O'Connell, 2000. SHETRAN: Distributed River Basin Flow and Transport Modeling System. J. Hydrologic Engineering, 5(3):250-258.

16. HydroGeoLogic, Inc., 2001. MOD-HMS: A Comprehensive MODFLOW-based Hydrologic Modeling System. Version 1.1. Document and Users Guide, HydrolGeoLogic Inc., Herndon, Virginia

17. VanderKwaak, J. E., 1999. Numerical Simulation of Flow and Chemical Transport in Integrated Surface-Subsurface Hydrologic Systems [InHM]. Ph.D. Thesis, Dept. of Earth Science, University of Waterloo, Waterloo, Ontario, Canada.

18. Wigmosta, M. S. and Perkins, 1997. A GIS-Based Modeling System for Watershed Analysis [GISWA]. Final Report to the National Council of the Paper Industry for Air and Stream Improvement. 160 pp.

19. South Florida Regional Simulation Model-Hydrologic Simulation Engine (SFRSM-HSE). http://www.sfwmd.gov/org/pld/hsm/models/sfrsm/index.html http://www.sfwmd.gov/org/pld/hsm/models/sfrsm/hse/hse.html.

20. Walton, R., E. J. Wexler and R. S. Chapman. 1999. An Integrated Groundwater / Open-Channel Flow Model. Technical Report, WEST Consultants, Inc., Bellevue, WA and Gartner Lee Ltd., Toronto Canada.

21. Maconald I., Baines, M.J., Nichols N.K. and Samuels P.G. (1997). Analytic Benchmark Solutions for Open-Channel Flows, Journal of Hydraulic Engineering, Vol. 123, No. 11, November, 1997.

22. CH_2M Hill, 1989. Construction of and Testing of the Aquifer Storage Recovery (ASR) Demonstration Project for Lake Okeechobee, Florida. South Florida Water Management District. Prepared by CH_2M Hill, 800 Fairway Drive, Suite 350, Deerfield Beach, Florida 33411.

23. Brown, L. C. and T. O. Barnwell, Jr., 1987. The Enhanced Stream Water Quality Models QUAL2E and QUAL2E-UNCAS: Documentation and User Manual. EPA/600/3-87/007. Environmental Research Laboratory, Office of Research and Development, U.S.E.P.A, Athens, GA 3061.

24. Ambrose, R.B., T.A. Wool, and J.L. Martin, 1993. The water quality analysis simulation program, WASP5 Water version 5.10. Part A: Model documentation. U.S. Environmental Protection Agency, Office of Research and Development, Environmental Research Laboratory, Athens, GA.

25. Cerco, C. E. and T. Cole, 1995. User's Guide to the CE-QUAL-ICM. Release Version 1.0. Technical Report EL-95-1. U.S. Army Engineer Waterways Experiment Stations, Vicksburg, MS.